A COMPARISON OF REDUCED AND FULL DIMENSIONAL SIMULATION MODELS FOR PROTON EXCHANGE MEMBRANE FUEL CELLS

Gwang-Soo Kim[1†], P.C. Sui[2‡] and Akeel Shah[3§]

[1] Ballard Power Systems, Burnaby BC, Canada
[2] Institute for Integrated Energy Systems, University of Victoria, Victoria BC, Canada
[3] Simon Fraser University, Burnaby BC, Canada

ABSTRACT

Transport phenomena in a proton exchange membrane fuel cell (PEMFC) are highly coupled and complicated by multi-phase flow in the several porous components, electrochemical reaction and the three-dimensional geometry. Naturally, therefore, theoretical work is largely manifested in computational fluid dynamics (CFD). However, the comprehensive three-dimensional (3D) CFD method is often prohibitively time-consuming and, consequently, is not yet a suitable basis for a screening tool that operates under a wide range of design options and operating conditions. Mathematical models and solution procedures using simplified models with reduced dimensions have been proposed to address the issue of CFD time expense. Such approaches are computationally efficient, but no systematic study has been conducted to quantitatively assess the effects of the neglected dimensionality. In this paper we compare 3D CFD models, for a straight unit cell, with a hierarchy of reduced-dimensional models. We demonstrate that the 2+1D approach is currently the optimal choice as the basis for a tool to assist MEA and unit-cell design in the early stages of a design cycle.

Keywords: Proton exchange membrane fuel cell, CFD, transport phenomena, reduced-dimensional, efficient simulation

INTRODUCTION

The past decade has seen fuel cells emerging as a feasible alternative power source because of their high power density and overall low emission when compared to conventional technologies. Proton exchange membrane fuel cells (PEMFCs), which operate at relatively low temperatures, have been under development for applications over a wide range of power output. The structure of a PEMFC is surprisingly simple compared to incumbent technologies, for example internal combustion engines: a typical "plate-and-frame" PEMFC consists of a membrane electrode assembly (MEA), a membrane sandwiched between catalyst layers and gas diffusion layers (GDL) on both sides, and bipolar plates that conduct electricity and provide flow pathways for the reactants and product water. Despite its simple structure, the transport phenomena in a proton exchange membrane fuel cell (PEMFC) are highly coupled. Transport of heat, charged species (ions and electrons) and non-charged species are intimately related,

---

which makes analysis and experimental studies difficult. This situation is further complicated by multi-phase flow in the several porous components, electrochemical reaction and the complex three-dimensional geometry. It is natural, therefore, that a great deal of the modeling effort fits into a computational fluid dynamics (CFD) framework, examples of which include [1-4]. However, the most comprehensive three-dimensional (3D) CFD methods can be extremely time-consuming, and therefore not suitable as a basis for efficient (accurate and expeditious) testing of design options under several operating conditions of interest – a typical industrial requirement. Mathematical models and solution procedures using simplified models with reduced dimensions have been proposed to address the issue of CFD time expense, for example [5-9]. Although these approaches lead to a reduction in the time cost, no systematic study has been conducted to quantitatively assess the effects of the neglected dimensionality. In this paper we compare 3D CFD models, for a straight unit cell, with a hierarchy of reduced-dimensional models, including

1. 2D (cross-section of gas channels and the MEA),
2. 2+1D, or pseudo-3D (cross-section of gas channels and MEA together with 1D down-channel).

Our objective is to propose a reduced-dimensional methodology that is capable of providing results with accuracy comparable to that of 3D CFD but at a fraction of the time cost. The same underlying governing equations and parameters are solved for all the models tested and in order that direct comparisons could be made, all calculations for reduced dimensional models were performed with the commercial software FEMLAB on the same computer hardware.

MATHEMATICAL FORMULATION

The governing equations solved in the present study are summarized in Table 1. In essence, conservation of mass, momentum, gas species, charged species (manifested as electrical potentials for protons and electrons separately) and energy is solved for the entire computational domain (see [10] for more details). The transport of water across the membrane is described by the phenomenological model of [11], which includes the mechanisms of diffusion and electro-osmotic drag. For simplicity, we assume a constant diffusion coefficient. A two-phase flow model for liquid water transport in porous media is included, based on that of [12]. Such a two-phase model is not implemented in the reduced models and the operation conditions for the baseline case are chosen to prevent condensation. A commercial software, CFD-ACE+ version 2004, was employed to perform all 3D simulations in the present study.

PSEUDO 3D MODEL AND NUMERICAL METHOD

Figure 1 depicts the computational domain of a straight, single channel unit cell used for the 3D CFD calculation and reduced dimensional study. At the gas channel inlets, the mass flow rate and mass fractions of the gas are specified based on a desired stoichiometric ratio and dew point. Except at the inlets and outlets shown in Fig. 1, zero-flux boundary conditions for mass, temperature and potential apply on all boundary faces.

The potential on the top and the bottom surfaces is varied. Because of the thin layer structure of the MEA and the imposed potential boundary conditions, it is expected that the gradient of the primary variables (concentration of gas species and potentials) are high in the direction perpendicular to the MEA (Y-coordinate). This direction is called the 'primary direction' in the present study. The gas mixtures in the anode and cathode flow in the axial direction (Z-coordinate). Under normal operating conditions the reactant concentrations exhibit significant variations between the inlet and outlet, due to consumption along the flow pathway. We call this direction the 'secondary direction'. In a number of reduced-dimensional studies, the transport in the lateral direction, i.e. X-coordinate, is assumed negligible, leading to the so-called 1+1D model. However, the transport in this direction is found to depend strongly on the channel spacing, [13], invalidating this assumption in some cases. Nevertheless, the 1+1D approximation greatly simplifies the numerical description, and quite often algebraic manipulation is feasible ([7,8]).

A similar treatment can be used to simplify the 3D simulation. For mass and charge transport the high aspect ratio of the PEMFC suggests that diffusion in Z direction (down the channel) is negligible compared to that in the X-Y plane. However, convective mass transport in this direction is dominant. Moreover, fluid flow in the channel can be approximated as a plug flow with velocity V. With this approximation, each of the cross-sections is coupled through convective transport in the channel. This is the so-called pseudo-3D or 2+1D model. In this work, the same set of governing equations is used to model both the 3D and pseudo-3D simulations.

The solution procedure for the reduced dimensional approach is described in Figure 2. In the co-flow case the anode and cathode flows are treated in the same fashion: starting from the inlet, concentrations are used as channel conditions, together with an applied voltage. Once the boundary-value problem converges, the local current density and the flux from the MEA to channel are recorded. A plug flow model in the channel is used to predict the channel concentration at the next nodal point. This procedure is repeated down the length of the channel. For the counter-flow case back-and-forth shooting is required since the anode and cathode flows are opposed. In the forward shooting, the anode concentration profile is fixed and the current distribution is calculated as in the co-flow case. Once the end of the channel is reached, the cathode concentration profile is fixed, and the anode concentration profile and current distribution are updated while marching in the backward direction. This iteration is repeated until the residual of the current distribution falls within a specified tolerance. A 2D cross-section was implemented with FEMLAB 3.1. The convective mass transport equation in the channel was solved using MATLAB.

RESULTS AND DISCUSSION

To assess the validity of the numerical implementation, polarization curves were constructed using 1D and 2D FEM models in Figure 3. The results were compared with those from a fully 3D model assuming short channels and a high stoichiometry to minimize variations in the z direction. The result matched very well for loads in the range 0-1A/cm^2. For loads greater than 1A/cm^2 the curves begin to diverge. For the 1D case, because it does not have the rib-channel geometry, the additional ohmic loss due to

presence of the rib (see [13]) is zero, hence resulting in a higher predicted cell potential. For the 2D case, although it resolves the rib-channel geometry, at high current density conditions, effects due to liquid water on mass transport, which is considered in the 3D CFD calculation, are not present, therefore a slightly higher cell potential is predicted.

A number of simulations were conducted to compare the different geometric approximations, with conditions as follows:

- Temperature =70 (inlet), 80ºC (outlet)
- C_{O2}: air composition
- Dew point 40ºC for both cathode and anode
- C_{H2}: pure hydrogen
- Φ_{O2}: stoichiometry of 5 for 1A/cm^2
- Φ_{H2}: stoichiometry of 5 for 1A/cm^2

To construct the entire polarization curve, the computation time for the 2D model is typically less than a few minutes, but generally the results do not match those of 3D CFD. However, it is possible to fit the 2D model results to the CFD results by tuning the mass transport coefficient (or Sherwood number Sh) at the interface between the MEA and channel. The 2+1D model fully resolves the cross-channel effects and includes convective mass transport in the channels. The typical computation is roughly 30 minutes on an Intel Pentium 4™ processor (2 GHz) and the results generally match very closely with those of 3D CFD, without the need of fitting parameters.

Figure 4 shows the comparison between 2D and 3D results. The top row of plots shows the sensitivity of current distribution for co-flow (Fig. 4(a)) and for counter-flow (Fig. 4(b)) to variations in Sh. It can be seen that the 2D result is very sensitive. With a typical value of Sh = 2 (laminar conditions), inlet and outlet current distributions are overpredicted for the co-flow case. With a very large Sh, in this case 100, a similar trend is observed. For the counter flow case, the same value of Sh generates a current distribution that is qualitatively different from the CFD result; in the latter, the current reaches a maximum in the first half of the cell, but with Sh = 2, the maximum reaches the second half of the cell. With Sh = 100, the current does not reach an interior maximum, but monotonically increases from inlet to outlet.

It must be stressed that in order to obtain agreement with the CFD result, the Sherwood number and voltage were adjusted so that the current density distributions matched. This iterative fitting procedure is inherently time consuming and is not well suited to the study of a large number of cases.

The solid curve in Figure 4 (a) and the symbols in Figure 4 (c) are the current density and RH profile with Sh = 0.34 and V = 0.47 V in the co-flow operation. The agreement between 2D and 3D is surprisingly good. However, the Sherwood number had to be fitted again to match 3D result in the counter-flow operation (see Figure (b) and (d)), now taking the value Sh = 0.46.

It is also worth noting that the fitted Sherwood numbers for co- and counter-flow are smaller than realistic values of around 2 (apart from being different for the co- and counter-flow cases). The 2D approximation underpredicts the mass transport resistance in the x direction (see Figure 1), since it assumes the width of the unit cell is the same as the width of the channel. A small Sherwood number accounts for this neglected mass transport resistance.

In principle, any additional mass transport in the x direction should be well captured in the 2+1D or pseudo 3D models. Figure 5 shows the comparison between the latter two. With a Sherwood number of 2, the qualitative trends are well matched, that is, without fitting. Although the cathode and anode (equilibrium) relative humidity is slightly over-predicted by the 2+1D results and the maximum in the current is shift slightly to the center in the counter-flow case, the profiles are in good qualitative agreement with the 3D result. In particular, this illustrates that the mass transport behavior of the 3D model is well approximated by the 2+1D approach.

In order to avoid the problems encountered in the 2D case we did not attempt to fit Sh to achieve a closer match with the CFD result. In fact, the 2+1D model without fitting captures the effects of important geometric factors including channel dimension, plate thickness and MEA thickness on the performance of the PEMFC.

CONCLUSION

The differences between 2D and 2+1D indicate that coupling between mass, heat and charge transport is important, particularly in the cross-channel direction. When mass transport of water is not captured well, the distribution of the hydration level along the channel is strongly affected, resulting in skewed current distributions.

It is encouraging that a 2D model can be calibrated to approximate the behavior in a real fuel cell geometry, but this comes at the cost of a rather time-consuming fitting procedure (Sh may also have to be re-fitted when operating conditions/configuration changes), which represents a critical limitation.

On the other hand, the 2+1D model reported in this paper has a greater computational efficiency than the comprehensive 3D CFD model with comparable accuracy and does not suffer from the problems encountered in the 2D case. The implication of this result is that the 2+1D approach is (currently) the optimal modeling tool for the extensive testing required in MEA and unit-cell design, particularly in the early stages of a design cycle.

ACKNOWLEDGEMENTS

NOMENCLATURE

C Molar concentration, mol/m^3
D_λ Water diffusion coefficient, mol/m s
f   F/RT
F   Faraday constant, 96487 C
h Mixture enthalpy, J/kg
h_i Enthalpy of i-th species, J/kg
i   Current density, A/m^2

J   Mass flux, kg/m^2-s

J_i Mass flux of i-th species, kg/m^2-s

j_0 Exchange current density, A/cm^2

j_T Transfer current density on catalyst, A/m^2

k   Thermal conductivity, W/m-K

M_m Equivalent weight of a dry membrane, kg/mol

N_G Number of gas-phase species

n_d Electro-osmotic drag coefficient, dimensionless

P   Pressure, Pa

RH   Relative humidity, dimensionless

$\dot{S}_h$ Enthalpy source due to phase change, W/m^3

$(S/V)_{eff}$ Effective surface to volume ratio, m^2/m^3

s   Saturation

T   Temperature, K

V   Cell voltage, Volt

$\vec{V}_i$ Diffusion velocity of species i, m/s

X   X-coordinate (between channel and landing)

Y   Y-coordinate (perpendicular to the MEA)

Y_i Mass fraction of i-th species

Z   Z-coordinate (axial)

Greek

α Transfer coefficient in Butler-Volmer equation

ε Wet porosity

ϕ Electrical potential, V

Φ Stoichiometric ratio

η Activation overpotential, V

γ Order of chemical reactions

κ_P Permeability, m^2

κ_{ce} Phase change rate, $1/s^2$-m^2

λ Water content, dimensionless

μ Dynamic viscosity, kg/m-s

ρ Density of mixture, kg/m^3

ρ_m Density of a dry membrane, kg/m^3

σ Electrical conductivity, S/m

$\bar{\bar{\tau}}$ Shear Stress tensor, N/m^2

Subscript

a   Anode side of the membrane

c   Cathode side of the membrane

H2   Hydrogen

O2   Oxygen

P   Pore

sat   Saturation

REFERENCES

1. Gurau V., Liu H. T. and Kakac S. "Two-dimensional model for proton exchange membrane fuel cells." AIChE Journal. 1998; 44(11): 2410-2422.

2. Berning T., Lu D. M. and Djilali N. "Three-dimensional computational analysis of transport phenomena in a PEM fuel cell." J. Power Sources. 2002; 106(1-2): 284-294.

3. Ju H. and Wang C. Y. "Experimental validation of a PEM fuel cell model by current distribution data." J. Electrochem. Soc. 2004; 151(11): A1954-A1960.

4. Dutta S., Shimpalee S. and Van Zee J. W. "Three-dimensional numerical simulation of straight channel PEM fuel cells." J. Applied Electrochem. 2000; 30(2): 135-146.

5. Yi J. S. and Nguyen T. V. "An along-the-channel model for proton exchange membrane fuel cells." J. Electrochem. Soc. 1998; 145(4): 1149-1159.

6. Kulikovsky A. A. "Quasi-3D modeling of water transport in polymer electrolyte fuel cells." J. Electrochem. Soc. 2003; 150(11): A1432-A1439.

7. Kulikovsky A. A. "1D+1D model of a DMFC: localized solutions and mixedpotential." Electrochem. Comm. 2004; 6(12): 1259-1265.

8. Berg P., Promislow K., St Pierre J., Stumper J. and Wetton B. "Water management in PEM fuel cells." J. Electrochem. Soc. 2004; 151(3): A341-A353.

9. Freunberger S. A., Santis M., Schneider I. A., Wokaun A. and Buchi F. N. "In-plane effects in large-scale PEMFCs - Model formulation and validation." J. Electrochem. Soc. 2006; 153(2): A396-A405.

10. Mazumder S. and Cole J. V. "Rigorous 3-d mathematical modeling of PEM fuel cells - I. Model predictions without liquid water transport." J. Electrochem. Soc. 2003; 150(11): A1503-A1509.

11. Springer T. E., Zawodzinski T. A. and Gottesfeld S. "Polymer Electrolyte Fuel-Cell Model." J. Electrochem. Soc. 1991; 138(8): 2334-2342.

12. Mazumder S. and Cole J. V. "Rigorous 3-d mathematical modeling of PEM fuel cells - II. Model predictions with liquid water transport." J. Electrochem. Soc. 2003; 150(11): A1510-A1517.

13. Sui, P.C. and Djilali, "Analysis of coupled electron and mass transport in the gas diffusion layer of a PEM fuel cell", J. Power Sources. 2006; in press.

Table 1. Governing equations

	Convection	Diffusion	Source
Mass	$\nabla \cdot (\varepsilon \rho \vec{V})$	-	$\dot{m}$
Momentum	$\nabla \cdot \left(\varepsilon \rho \vec{V} \vec{V} \right)$	$-\nabla P + \nabla \cdot (\varepsilon \bar{\tau})$	$-(\varepsilon^2 \dfrac{\mu}{k_p}) \vec{V}$
Energy	$\nabla \cdot \left(\varepsilon \rho \vec{V} h \right)$	$\nabla \cdot (k \nabla T + \sum\limits_{i=1}^{N_G} \vec{J}_i h_i)$	$\varepsilon \bar{\tau} : \nabla \vec{V} + \varepsilon \dfrac{dP}{dt} + \dfrac{\left| \vec{i} \cdot \vec{i} \right|}{\sigma} - j_T \eta + \dot{S}_h$
Species	$\nabla \cdot (\varepsilon \rho \vec{V} Y_i)$	$\nabla \cdot \vec{J}_i{}^*$	$\rho D_i \dfrac{Y_i - Y_{P,i}}{\delta} \left(\dfrac{S}{V} \right)_{eff}$
Potential	-	$\nabla \cdot (\sigma_k \nabla \phi_k)$	$j_{0,k} (\dfrac{c_k}{c_{k,ref}})^{\gamma_k} \cdot (e^{\alpha_{a,k} f \eta} - e^{-\alpha_{c,k} f \eta}) \cdot \left(\dfrac{S}{V} \right)_{eff}$
Saturation	$\nabla \cdot (\rho_l \vec{V} s)$	$\nabla \cdot [\dfrac{\rho_l K s^3}{\mu_l} \dfrac{dp_c}{ds} \nabla s]$	$r_w{}^{**}$
Water content	$\nabla \cdot (\dfrac{n_d}{F} \vec{i})$	$-\dfrac{\rho_m}{M_m} \nabla \cdot (D_\lambda \nabla \lambda)$	-

$* \quad \vec{J}_i = \rho D_i \nabla Y_i + \dfrac{\rho Y_i}{M} D_i \nabla M - \rho Y_i \sum\limits_j D_j \nabla Y_j - \dfrac{\rho Y_i \Delta M}{M} \sum\limits_j D_j Y_j$

$** \quad r_w = \kappa_{c,e} \cdot (x_w P - P_{sat})$
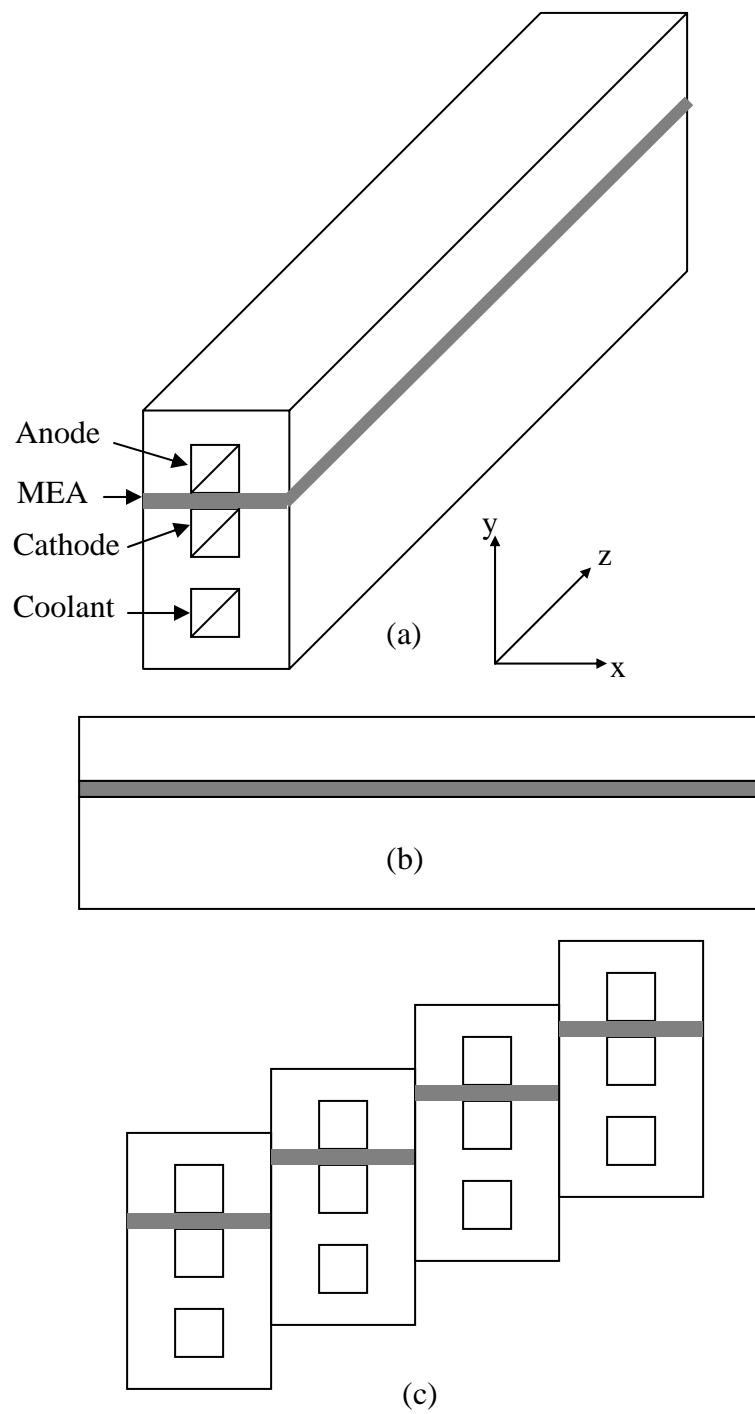
Figure 1. Geometry approximation: (a) 3D geometry, (b) 2D geometry (c) pseudo 3D geometry
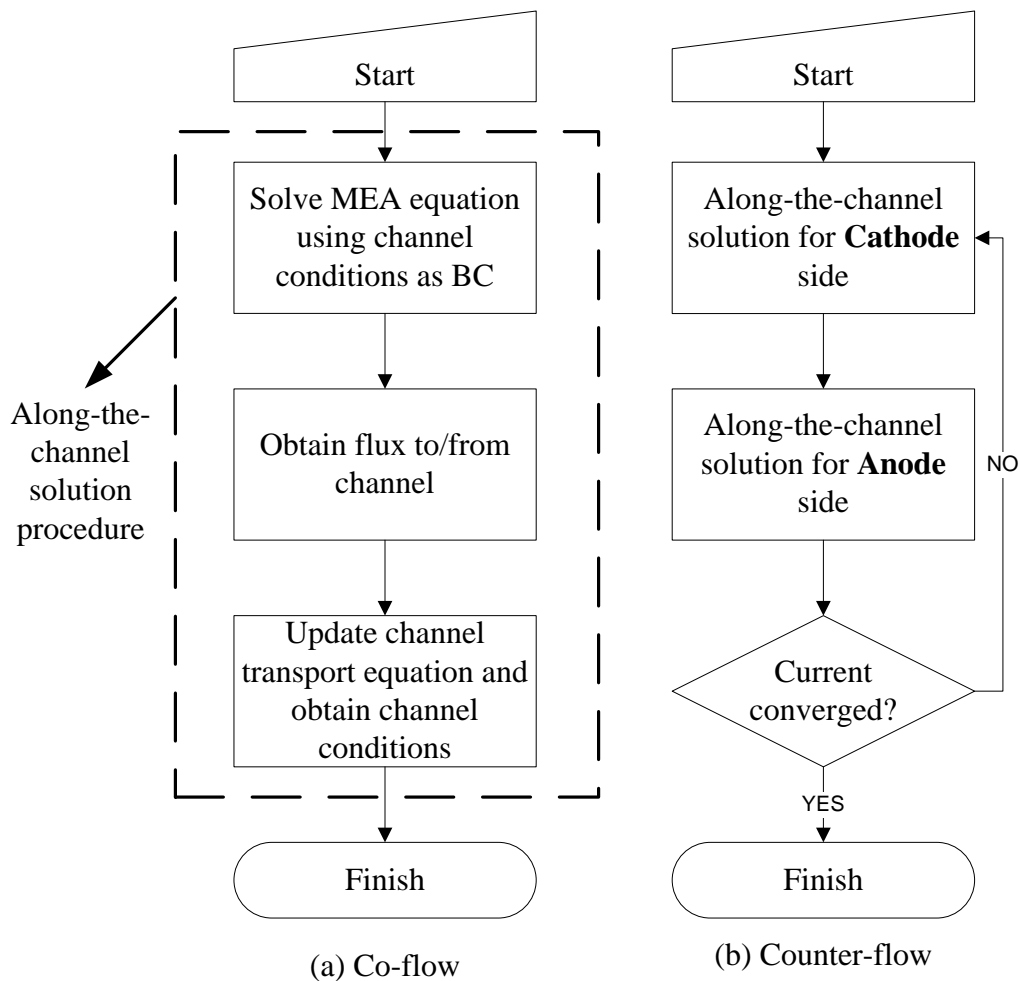
Figure 2. Flow chart depicting the code methodology: (a) co flow (b) counter flow
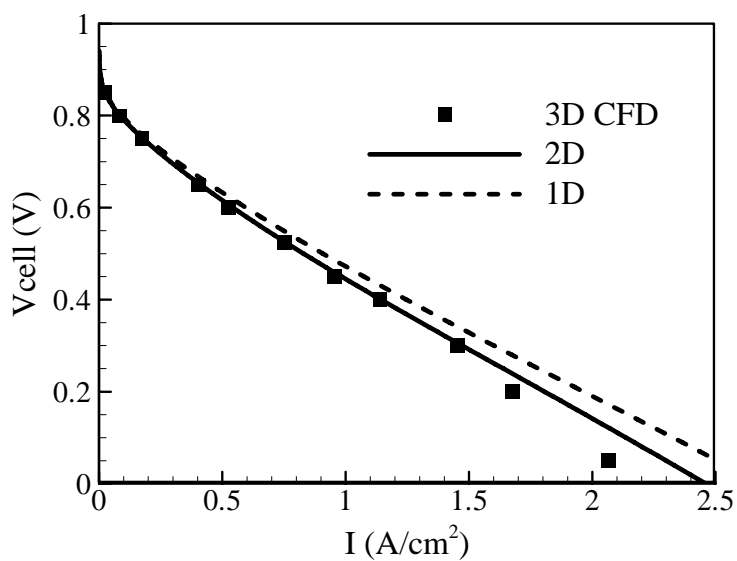
Figure 3. A comparison between the 1D, 2D and 3D results.
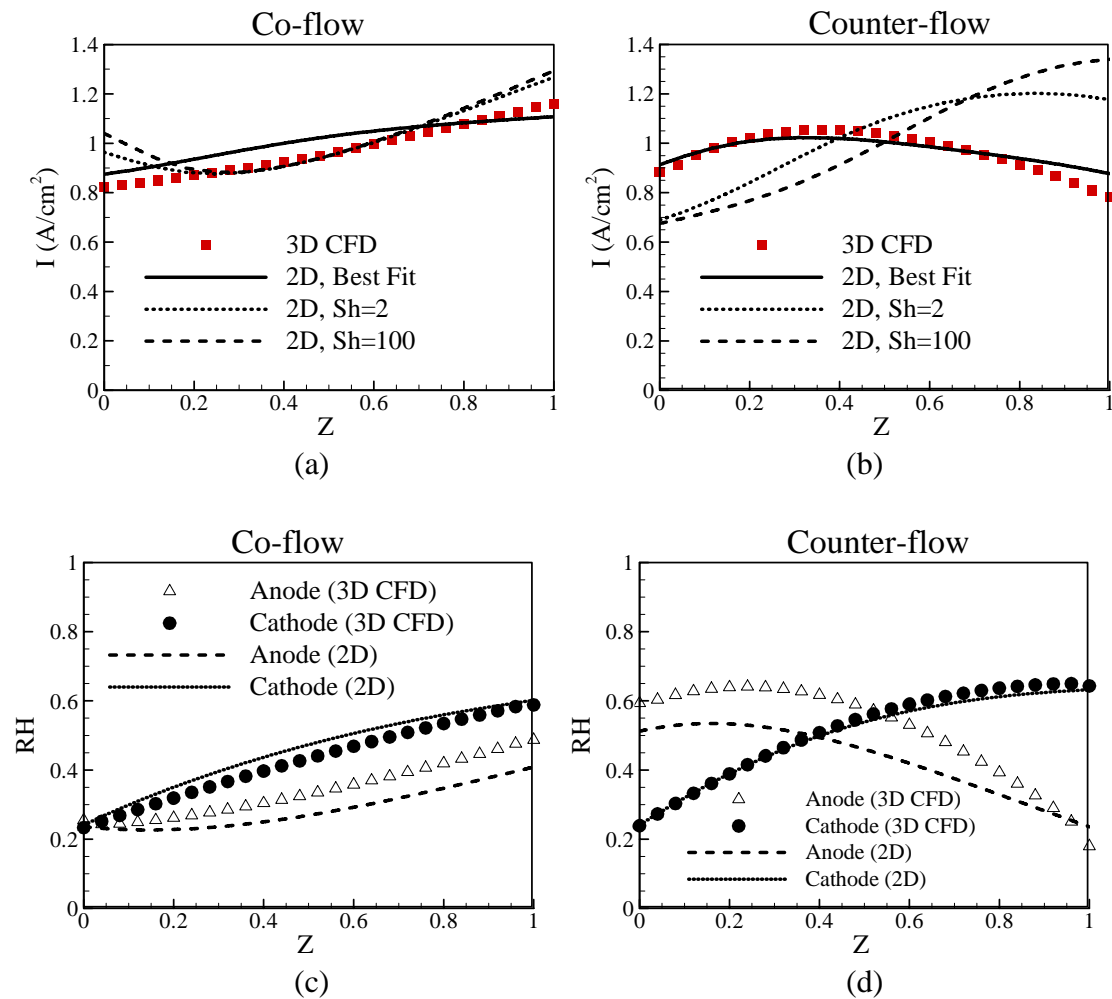
Figure 4. A comparison of 2D and 3D CFD results: I for (a) co-flow and (b) counter-flow; RH for (c) co-flow and (d) counter-flow.
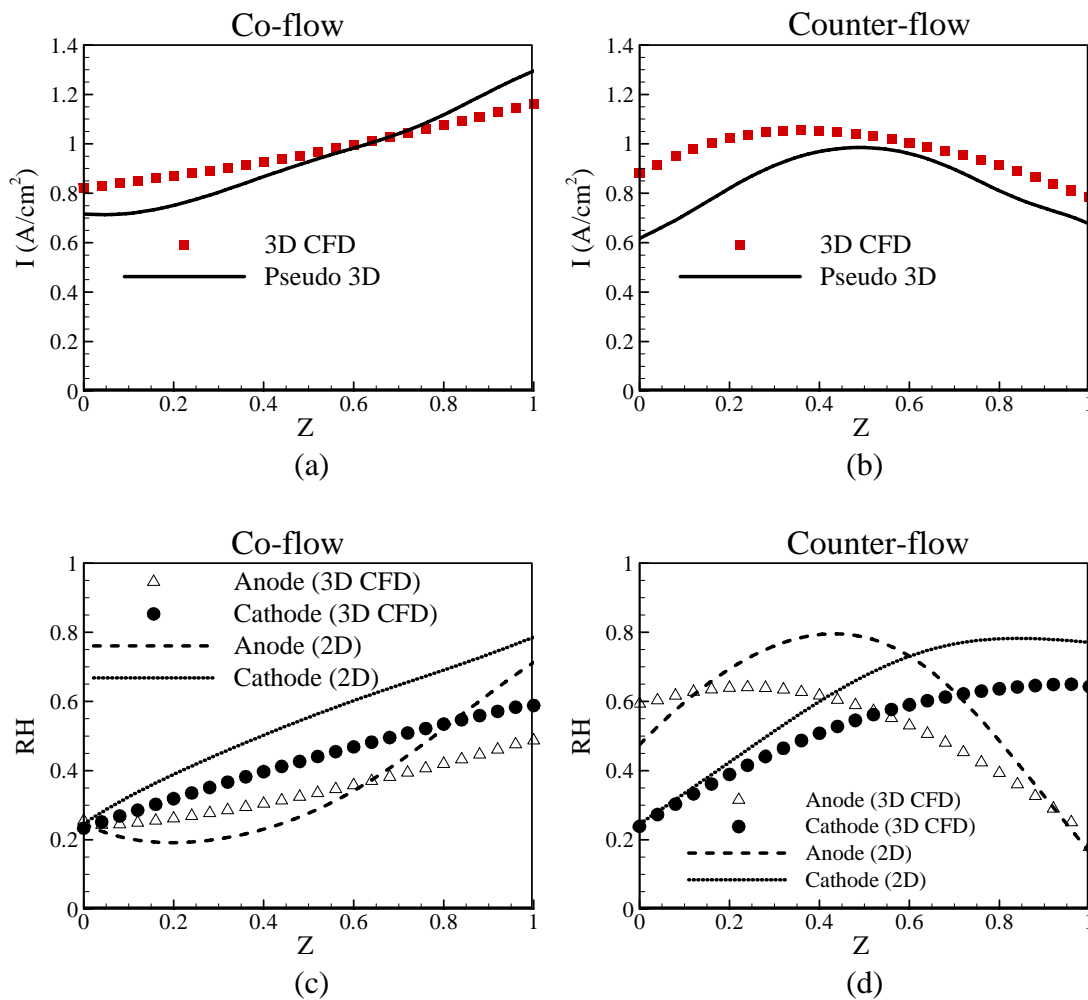
Figure 5. A comparison of pseudo 3D and 3D CFD results: I for (a) co-flow and (b) counter-flow; RH for (c) co-flow and (d) counter-flow